

Constraining the particle-scale diversity of black carbon light absorption using a unified framework

Payton Beeler and Rajan K. Chakrabarty

Center for Aerosol Science and Engineering, Department of Energy, Environmental and Chemical Engineering, Washington University in St. Louis, St. Louis, MO 63130

Correspondence: Rajan Chakrabarty (chakrabarty@wustl.edu) and Payton Beeler (beelerpayton@wustl.edu)

Abstract. Atmospheric black carbon (BC), the strongest absorber of visible solar radiation in the atmosphere, manifests across a wide spectrum of morphologies and compositional heterogeneity. Phenomenologically, the distribution of BC among diverse particles of varied composition gives rise to enhancement of its light absorption capabilities by over twofold in comparison to

that of nascent or unmixed homogeneous BC. This situation has challenged the modeling community to consider the full complexity and diversity of BC on a per-particle basis for accurate estimation of its light absorption. The conventionally adopted core-shell approximation, although computationally inexpensive, is inadequate in not only estimating but also capturing absorption trends for ambient BC. Here we develop a unified framework that encompasses the complex diversity in BC morphology and composition using a single metric, the phase shift parameter (ρ_{BC}), which quantifies how much phase

shift the incoming light waves encounter across a particle compared to that in its absence. We systematically investigate variations in ρ_{BC} across the multi-space distribution of BC morphology, mixing-state, mass, and composition as reported by field and laboratory observations. We find that $\rho_{BC} > 1$ leads to decreased absorption by BC, which explains the weaker absorption enhancements observed in certain regional BC compared to laboratory results of similar mixing state. We formulate universal scaling laws centered on ρ_{BC} and provide physics-based insights regarding core-shell approximation overestimating

BC light absorption. We conclude by packaging our framework in an open-source Python application to facilitate community-level use in future BC-related research. The package has two main functionalities. The first functionality is for forward problems, where experimentally measured BC mixing state and assumed BC morphology are input, and the aerosol absorption properties are output. The second functionality is for inverse problems, where experimentally measured BC mixing state and absorption are input, and the morphology of BC is returned. Further, if absorption is measured at multiple wavelengths, the package facilitates the estimation of imaginary refractive index of coating materials by combining the forward and inverse procedures. Our framework thus provides a computationally inexpensive source for calculation of absorption by BC, and can be used to constrain light absorption throughout the atmospheric lifetime of BC.

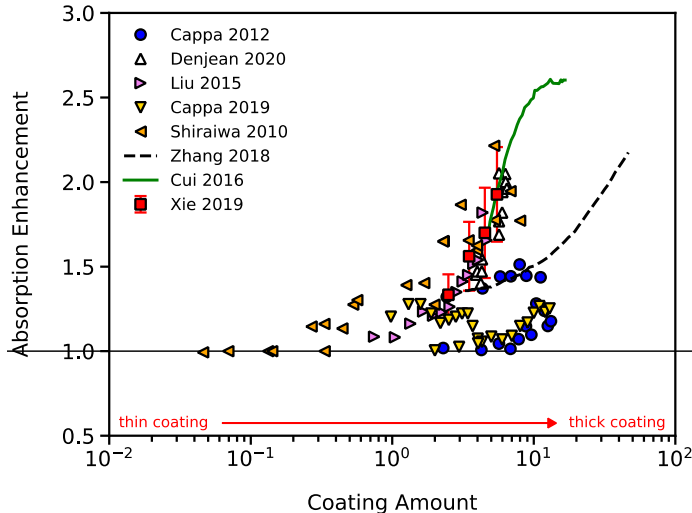
1 Introduction

30 The contribution of aerosols to global radiative forcing remains one of the largest sources of uncertainty in current climate models (Reidmiller et al., 2018). Much of this uncertainty stems from disagreements between the predicted and observed radiative forcing by carbonaceous aerosols (Bond et al., 2013; Gustafsson and Ramanathan, 2016; Boucher et al., 2016). One of the most climatically relevant carbonaceous aerosols is black carbon (BC). Black carbon is widely considered to be a predominate light absorbing atmospheric constituent (Bond et al., 2013; Bond and Bergstrom, 2006). Despite this, light
35 absorption by BC is still significantly underestimated in current climate models, which stems from incorrect parameterization of BC optical properties (Bond et al., 2013; Gustafsson and Ramanathan, 2016; Boucher et al., 2016). Estimation of BC light absorption is particularly complicated, given that BC is often internally mixed with other species, which manifest as external coatings (China et al., 2013).

External coatings enhance light absorption by BC through a “lensing effect”, in which a portion of the incoming light is
40 scattered by the coating into the BC core, where it is then absorbed (Chakrabarty and Heinson, 2018; Cappa et al., 2012; Peng et al., 2016; Saliba et al., 2016; Liu et al., 2017; Shiraiwa et al., 2010). However, previous studies on light absorption enhancement due to the lensing effect have had various results. Some studies find high absorption enhancement (up to a factor of 2.5), while others find little to no absorption enhancement with increasing coating amount (Cappa et al., 2012; Saliba et al., 2016; Shiraiwa et al., 2010; Liu et al., 2015; Cappa et al., 2019; Zhang et al., 2018; Denjean et al., 2020; Zanatta et al., 2018;
45 Xie et al., 2019; Cui et al., 2016). The range of absorption enhancement from previous studies is evident in Figure 1. Fierce *et al.* found that particle-to-particle heterogeneity reconciles a large portion of the observed discrepancies in light absorption enhancement (Fierce et al., 2020). However, even when particle-to-particle heterogeneity is considered, light absorption enhancement is still overestimated, and previous discrepancies cannot be fully resolved. Fierce *et al.* have also shown that representation of the complex morphology of BC further improves estimation of its optical properties, but systematic
50 understanding of the effect of BC morphology on light absorption enhancement is understudied.

Here, we take a two-pronged approach to develop a simple yet rigorous unified framework for parameterizing the effects of particle size, morphology, and mixing state on BC light absorption. The first approach involves reducing the aforementioned multivariate space to a single parameter that captures causal relationships between BC’s physio-chemical properties and corresponding light absorption. Using this parameter, we next develop universal scaling laws for wavelength-dependent BC
55 light absorption as a function of size, morphology, and mixing state. Previously, one would need to make assumptions regarding the morphology of BC, then select an appropriate model to calculate its light absorption properties. Our model is the first to allow for quick calculation of BC optical properties with any morphology. We validate these laws against observational datasets from eleven field campaigns which investigated global trends in BC absorption, as well as laboratory experiments that investigated light absorption enhancement. From the standpoint of practical applications of our framework, we package our
60 scaling laws into an open-source python software which allows researchers to use our results to estimate absorption of BC

aerosols based on their size, morphology, and mixing state, and also estimate the morphology of BC aerosols based on their size, absorption, and mixing state.



65 **Figure 1:** Results from previous studies on light absorption enhancement. Some studies find high absorption enhancement, which have had large discrepancies. Some studies find that absorption is enhanced by over twofold, while other studies find little to no absorption enhancement with increased coating amount (Cappa et al., 2012; Denjean et al., 2020; Liu et al., 2015; Cappa et al., 2019; Shiraiwa et al., 2010; Zhang et al., 2018; Cui et al., 2016; Xie et al., 2019).

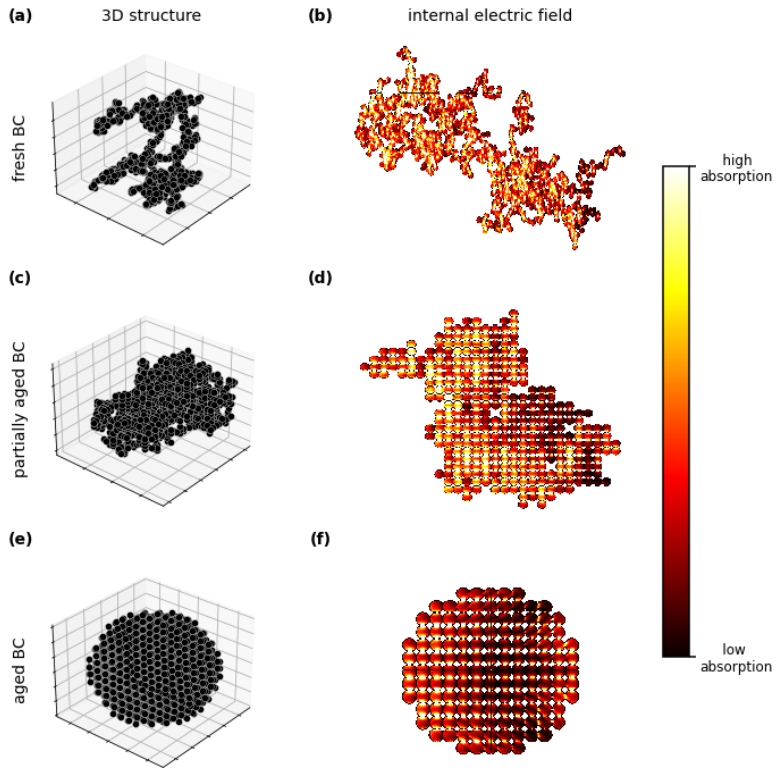
2 Methods

2.1 Representation of diverse black carbon morphologies

70 Black carbon is often modeled assuming a spherical core-shell configuration. However, soon after emission, BC aggregates have been found to have a lacy, fractal-like structure. Surface tension and capillary forces from the buildup of external coatings can cause BC aggregates to collapse, and eventually take on a more spherical structure (China et al., 2013; Liu et al., 2017; Fierce et al., 2020; Wang et al., 2017). Recent studies have found that non-sphericity of BC containing particles (partial encapsulation of BC) can decrease absorption enhancement (Hu et al., 2022, 2021). While these findings are notable, previous
75 studies have not observed a prevalence of partially-encapsulated BC, yet decreased light absorption enhancement is still observed (China et al., 2013; Fierce et al., 2020). Therefore, this study is focused on investigating the effects of core restructuring on light absorption enhancement, rather than the effects of partial BC encapsulation.

To model the evolution of BC morphology, we utilize three aggregation models which represent fresh, partially collapsed, and fully collapsed BC aggregates. Fresh BC aggregates were created using an off-lattice diffusion-limited cluster-cluster
80 aggregation model, which has been shown to accurately represent BC aggregates produced by combustion systems, and have a fractal dimension (D_f) of 1.83 ± 0.09 (Meakin, 1983, 1987). Partially and fully collapsed BC aggregates were respectively

simulated with a percolation model and simple cubic lattice stacking, and have D_f of 2.11 ± 0.22 and 3.0. These particles resemble electron microscope images of moderately and heavily coated BC, respectively (Fierce et al., 2020). Each simulated BC particle is comprised of monomers with radius equal to 20 nm (Bond et al., 2013). The amount of coating was quantified by the ratio of coating mass to BC mass (R_{BC}). Under this definition, increased R_{BC} represents increasing coating amount, and $R_{BC} = 0$ represents pure BC. The mass of the BC core and the coating material were determined per their volume and densities, 1.8 g/cm³ and 1.2 g/cm³, respectively (Bond and Bergstrom, 2006). This study utilized 345 aggregates, with BC masses between ~ 1 fg and ~ 70 fg, gyration radius between ~ 50 nm and ~ 300 nm, and R_{BC} between 0 and 49. Figure 2 shows examples of simulated aggregates, which represent the range of observed BC morphology.



90

Figure 2: The first column shows examples of 3D structure of (a) freshly emitted (b) partially aged and (c) aged black carbon (BC) particles, which represent the range of BC morphology observed during atmospheric processing in field and laboratory studies. The second column shows internal light absorption distribution across these aggregates, with light incident from the left of the particle. As BC becomes more compact, areas of decreased light absorption begin to emerge in the interior of the aggregate, which in turn leads to decreased MAC_{BC} .

95 **2.2 Calculation of optical properties**

The optical properties of the generated aggregates were calculated using the Amsterdam Discrete Dipole Approximation (ADDA 1.3b4) algorithm (Yurkin and Hoekstra, 2011). The ADDA algorithm operates by breaking complex shapes into sub-volumes which are small enough compared to the wavelength of light to be treated as point scatterers which interact with surrounding point scatterers. It is recommended that the wavelength of light be at least 10 times the size of individual sub-volumes in order for accurate calculation of optical properties. For this study, the wavelength of light was approximately 100 times the size of individual sub-volumes in order to reduce errors in calculation of optical properties. The ADDA algorithm calculated the absorption cross-section of each aggregate, which was then divided by the mass of the BC core to give mass absorption cross-section (MAC_{BC}) of each aggregate. Much of the previous work which investigates light absorption by internally mixed BC measure absorption enhancement (E_{abs}). Absorption enhancement is commonly defined as absorption by internally mixed BC divided by absorption by pure BC (Fierce et al., 2020). There are three common methods for estimating light absorption by pure BC: direct measurement (using thermodenuders to remove coating material), extrapolation of best fit lines of light absorption by internally mixed BC, and using literature values. All of these methods have challenges which can ultimately affect the reported value of E_{abs} . It has been found that thermodenuders may not remove low-volatility coating material, which leads to overestimation of light absorption by pure BC and underestimation of E_{abs} (Shetty et al., 2021).
100
105
110
115

Extrapolation of absorption measurements by internally mixed BC either assume that the morphology of BC does not affect light absorption, or that the morphology of BC remains fixed as coating accumulates. Finally, use of literature values to approximate light absorption by pure BC assumes that light absorption by fractal aggregates is equivalent to literature values of absorption by bulk BC. Rayleigh-Debye-Gans approximation of light absorption by fractal BC is significantly lower than commonly used literature values of absorption by pure BC (Bond and Bergstrom, 2006; Sorensen, 2001), indicating that use of literature values can also underestimate E_{abs} .

In order to avoid the errors associated with measurement of E_{abs} , we instead focus our efforts on quantification of MAC_{BC} . Absorption cross-section per BC mass is a common input of radiative transfer algorithms, and is vital in converting BC mass concentration to absorption coefficient (Bond et al., 2013). Accurate scaling of MAC_{BC} as a function of aggregate size, morphology, and mixing state will allow for subsequent calculation of E_{abs} which accounts for the evolution of BC morphology throughout its atmospheric lifetime.
120

2.3 Phase shift parameter is a unifying measure of size, morphology, and composition

Previous studies of E_{abs} have focused on the effects of a single dependent variable (absorption) as a function of a single independent variable (mixing state). However, detailed representation of the microphysical properties of BC leads to the introduction of several other measures which describe the size and morphology of BC, increasing the size of the variable set from two (absorption and mixing state) to four (size, morphology, absorption, and mixing state).
125

To reduce the size of the variable set, we utilize the phase shift parameter (ρ), which is a unifying measure of both aggregate size and morphology. Physically, ρ describes the amount of phase shift that light accumulates when passing through a particle (Heinson and Chakrabarty, 2016; Sorensen and Fischbach, 2000). When ρ is less than one, there is not a significant amount of phase shift in the incident wave, and the particle-light interactions are well described by Rayleigh approximations.

130 Conversely, when ρ is greater than one, the particle-light interactions are well described by geometric optics (Sorensen and Fischbach, 2000). In this work, ρ is used to describe the size and morphology of the BC core, not the entire particle (BC core + coating). Therefore, in the remaining text we refer to the core phase shift parameter (ρ_{BC}) to distinguish from the phase shift parameter of the entire particle. The core phase shift parameter is given by (Debye, 1958)

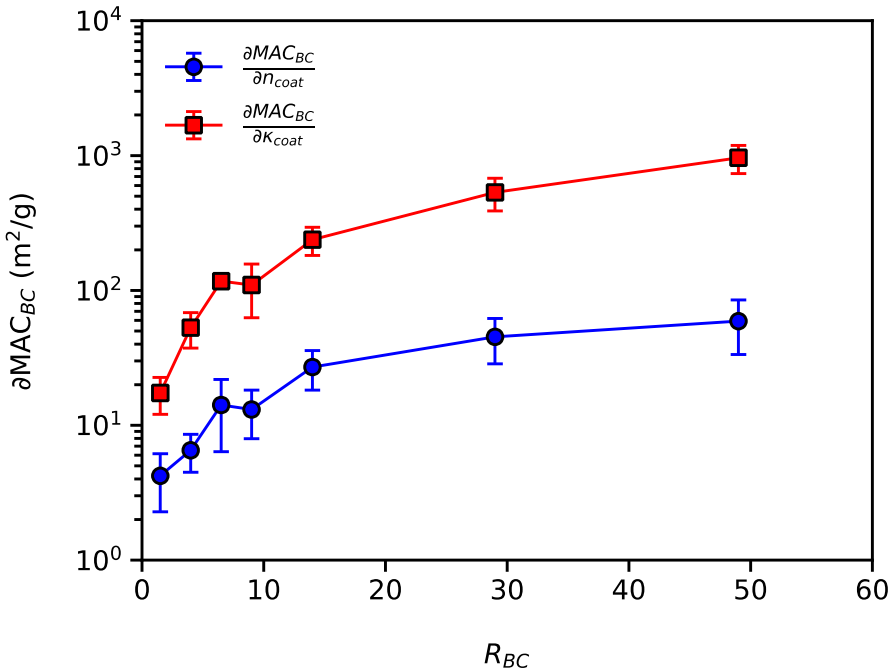
$$\rho_{BC} = \frac{4\pi R_g}{\lambda} |m_{eff} - 1|, \quad (1)$$

135 Where λ is the wavelength of incident light, R_g is the particle radius of gyration (size metric), and m_{eff} is the effective complex index of refraction, which in turn is given by

$$\phi \left(\frac{m^2 - 1}{m^2 + 2} \right) = \left(\frac{m_{eff}^2 - 1}{m_{eff}^2 + 2} \right). \quad (2)$$

Here, ϕ is the BC monomer packing fraction and m is the BC complex refractive index. The BC refractive index is fixed at 1.95+0.79i at all wavelengths (Bond and Bergstrom, 2006). The BC monomer packing fraction was calculated as the volume 140 of BC which lies within a sphere of radius R_g (centered at the center of mass) divided by the volume of a sphere with radius R_g . It is important to note that all parameters used in equation 1 and 2 describe the BC core, not the entire particle. It is also important to note that the dynamic compositional changes which a BC particle undergoes during atmospheric processing are captured by m_{eff} in equation 2 (Heinson et al., 2017). As coating accumulates on the surface of aggregates, the BC core will begin to collapse due to surface tension and capillary forces, and ϕ will increase. This will affect m_{eff} and eventually ρ_{BC} . The 145 aggregates in this study have ϕ between 0.029 and 0.52, representing the range observed in coated aggregates (Zangmeister et al., 2014; Chen et al., 2018). In general, for aggregates with equal size parameter, higher ϕ leads to higher ρ_{BC} . A plot of ρ_{BC} normalized by size parameter can be found in supplementary figure S1.

The consequence of increased ρ_{BC} on light absorption can be seen in Figure 2(b), (d), and (f), which show internal fields of the BC aggregates shown in Figure 1(a), (c), and (e). For fresh aggregates (with $\rho_{BC} \ll 1$), light is able to fully illuminate the 150 aggregate, and the entire volume contributes to light absorption. However, for fully collapsed aggregates (with $\rho_{BC} > 1$), light is not able to illuminate the far interior of the particle, leading to areas of decreased light absorption. Therefore, if ρ_{BC} of a particle significantly increases, its light absorption properties will change significantly. It should be noted that since ρ_{BC} is a function of both morphology and size of aggregates, full core collapse will not always lead to $\rho_{BC} > 1$. Aggregates with a small number of monomers may never achieve $\rho_{BC} > 1$, even when the monomer packing fraction reaches unity.

3.1 Sensitivity of MAC_{BC} to coating refractive index

160 **Figure 3:** Average change in MAC_{BC} per change in coating real refractive index ($\partial MAC_{BC}/\partial n_{coat}$) and average change in MAC_{BC} per change in coating imaginary refractive index ($\partial MAC_{BC}/\partial \kappa_{coat}$) with constant ϕ . We find that $\partial MAC_{BC}/\partial \kappa_{coat}$ is from 4 to 16 times greater than $\partial MAC_{BC}/\partial n_{coat}$, depending on R_{BC} . These results imply that the choice of coating imaginary refractive index is more important than the choice of coating real refractive index when calculating MAC_{BC} . Error bars represent one standard-deviation.

165 To examine the effects of coating refractive index, we calculate MAC_{BC} of 30 randomly selected BC aggregates with coating real refractive index (n_{coat}) of 1.45, 1.55, and 1.65, and coating imaginary refractive index (κ_{coat}) of 0.00, 0.05, and 0.1. Figure 3 shows the partial derivative of MAC_{BC} with respect to n_{coat} ($\partial MAC_{BC}/\partial n_{coat}$) and with respect to κ_{coat} ($\partial MAC_{BC}/\partial \kappa_{coat}$), with constant ϕ . We find that $\partial MAC_{BC}/\partial \kappa_{coat}$ is always greater than $\partial MAC_{BC}/\partial n_{coat}$, and increases with increased R_{BC} . These results show that the choice of κ_{coat} is more important than the choice of n_{coat} when calculating MAC_{BC} . Given this, we further investigate scaling of MAC_{BC} with κ_{coat} between 0.00 and 0.05, but n_{coat} remained fixed at 1.55 (Bond and Bergstrom, 2006).
170 In the context of field and laboratory measurements, particles with $\kappa_{coat} = 0.00$ are representative of BC which is internally mixed with non-refractory material, such as α -pinene secondary organic aerosol and sulfuric acid (Fierce et al., 2020). Particles with $\kappa_{coat} > 0.00$ are representative of BC which is internally mixed with absorbing material, such as brown carbon (Liu et al., 2015; Lu et al., 2015).

3.2 Phase shift parameter controls light absorption

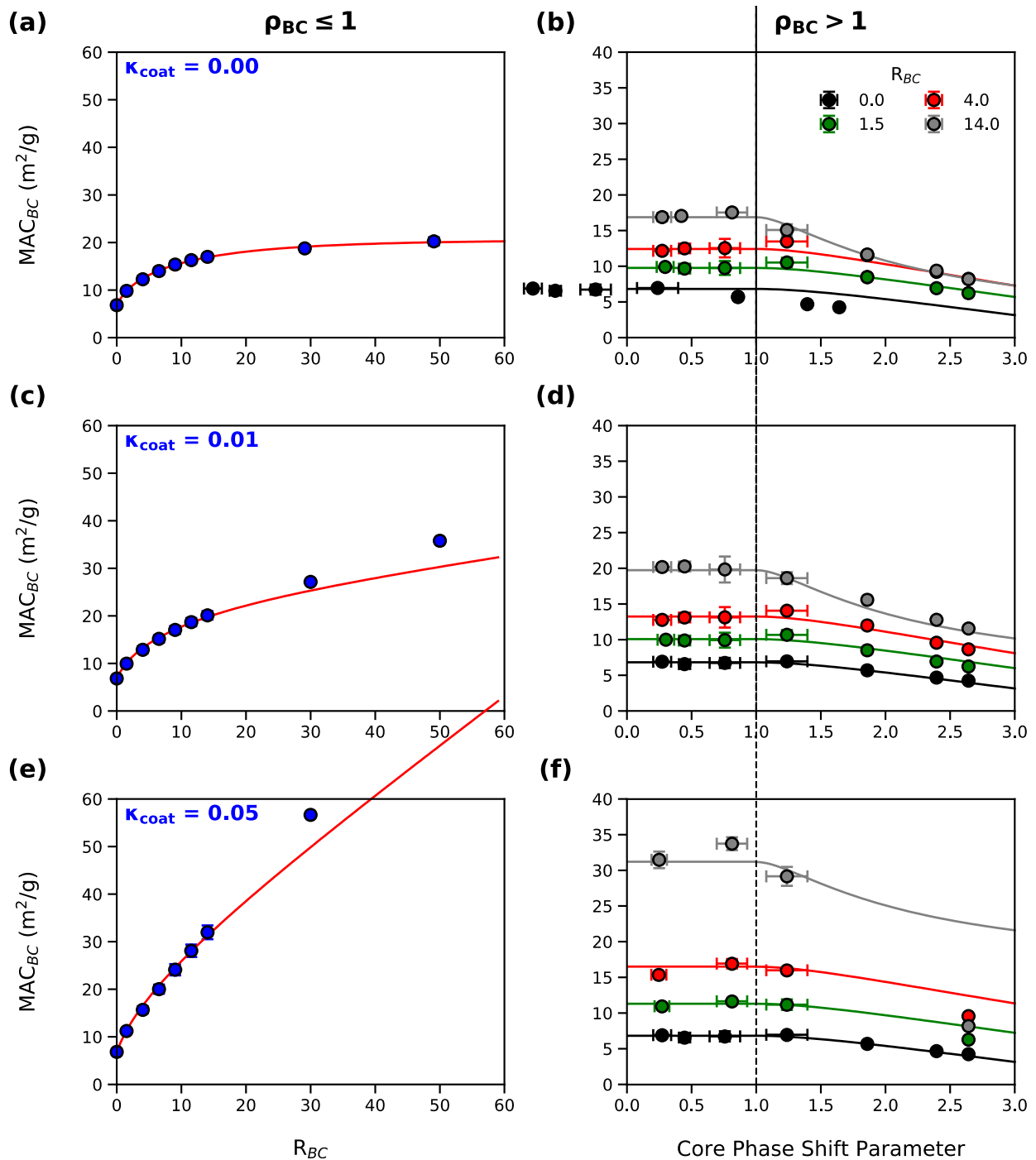
175 Figure 4 shows MAC_{BC} as a function of ρ_{BC} and R_{BC} for incident wavelength (λ) of 532 nm. Panels b, d, and f of Figure 4 show the clear emergence of two regimes separated by $\rho_{BC} = 1$ (dashed line). For $\rho_{BC} \leq 1$, MAC_{BC} increases with increased R_{BC} , but is independent of ρ_{BC} . For $\rho_{BC} > 1$, MAC_{BC} decreases with increased ρ_{BC} , and the rate of decrease is dependent on R_{BC} . The finding of decreased light absorption for $\rho_{BC} > 1$ is consistent with a recent study which also found decreased MAC_{BC} with increasing aggregate size (Romshoo et al., 2021). Best-fit lines for the scaling of MAC_{BC} as a function of R_{BC} are shown
180 as solid lines in Figure 4, and are summarized by

$$MAC_{BC} = \begin{cases} MAC_0 \left(\frac{\lambda}{\lambda_0} \right)^{-AAE} \left\{ \frac{1}{C} [AC^{-B} \Gamma(B+1, C)] - 2 - \frac{1}{C} [A(R_{BC} + 1)^B (C(R_{BC} + 1))^{-B} \Gamma(B+1, C(R_{BC} + 1))] + 3\kappa_{coat}(R_{BC} + 1) \right\}, & \rho_{BC} \leq 1 \\ MAC_0 \left(\frac{\lambda}{\lambda_0} \right)^{-AAE} \left\{ \frac{D}{E-1} \left[\left(\frac{1}{\rho_{BC}} \right)^{E-1} - 1 \right] + \frac{D}{1-2E} \left[\left(\frac{1}{\rho_{BC}} \right)^{2E-1} - 1 \right] \right\} + MAC_{BC}(R_{BC}, \rho_{BC} \leq 1), & \rho_{BC} > 1 \end{cases} \quad (3a)$$

Where A, B, and C are constants, Γ is the incomplete gamma function, and κ_{coat} is the imaginary part of the coating refractive index. The fitting parameters D and E are functions of R_{BC} , given by
185

$$X = x_1 + \frac{x_2 - x_1}{1 + \exp[x_3(R_{BC} - x_4)]}. \quad (4)$$

Where X generically represents D or E, and $x_{[1,2,3,4]}$ denotes $d_{[1,2,3,4]}$ or $e_{[1,2,3,4]}$. Finally, MAC_0 is the average MAC_{BC} at $\lambda = 532$ nm of uncoated aggregates with $\rho_{BC} \leq 1$ ($6.8 \text{ m}^2/\text{g}$) and AAE is the absorption Angstrom exponent for pure BC (1.158). The value of all constants used in equations 3 and 4 can be found in Table 1. Details regarding the acquisition of AAE can be found in supplementary figure S2.
190



195 **Figure 4.** Data and fitting of MAC_{BC} as a function of ρ_{BC} and R_{BC} for BC internally mixed with coating imaginary refractive index (κ_{coat}) of 0.00 (a-b), 0.01 (c-d), and 0.05 (e-f). We find that for constant ρ_{BC} , MAC_{BC} increases with increasing R_{BC} . Additionally, for constant R_{BC} , MAC_{BC} decreases when ρ_{BC} surpasses unity. Solid lines show scaling of MAC_{BC} given by equation 3.

We find AAE which is consistent with previously reported values (Bond et al., 2013; Romshoo et al., 2021), and fitting parameter B which is consistent with a previous numerical study of coated BC aggregates with $\rho_{BC} \leq 1$ (Chakrabarty and Heinson, 2018). The value of MAC_0 is less than commonly used literature values of pure BC ($7.75 - 8.0 \text{ m}^2/\text{g}$) (Bond et al., 2013; Liu et al., 2020), but slightly greater than Rayleigh-Debye-Gans approximation for MAC_{BC} , which accounts for the fractal morphology of BC ($5.01 \text{ m}^2/\text{g}$) (Sorensen, 2001). Figure 5(a) shows residual plots for the fitting of MAC_{BC} using equation 3. On average, equation 3 overestimates MAC_{BC} at $\lambda = 532 \text{ nm}$ by 0.47%, with standard deviation of 8.26%.
 205 Generally, relative errors increase as R_{BC} increases, as shown by Figure 5(b). It should also be noted that for thickly coated aggregates with $\kappa_{coat} > 0.00$, the scaling laws given in this work overestimate MAC_{BC} for aggregates with large ρ_{BC} , and slightly underestimate MAC_{BC} for aggregates with $\rho_{BC} < 1$. Underestimation of MAC_{BC} for large ρ_{BC} is likely due to accumulation of phase shift in the incident light as it passes through the coating material. This finding indicates that the scaling laws given by equation 3 are valid only when it can be assumed that the phase shift as light passes through coating materials is negligible.
 210

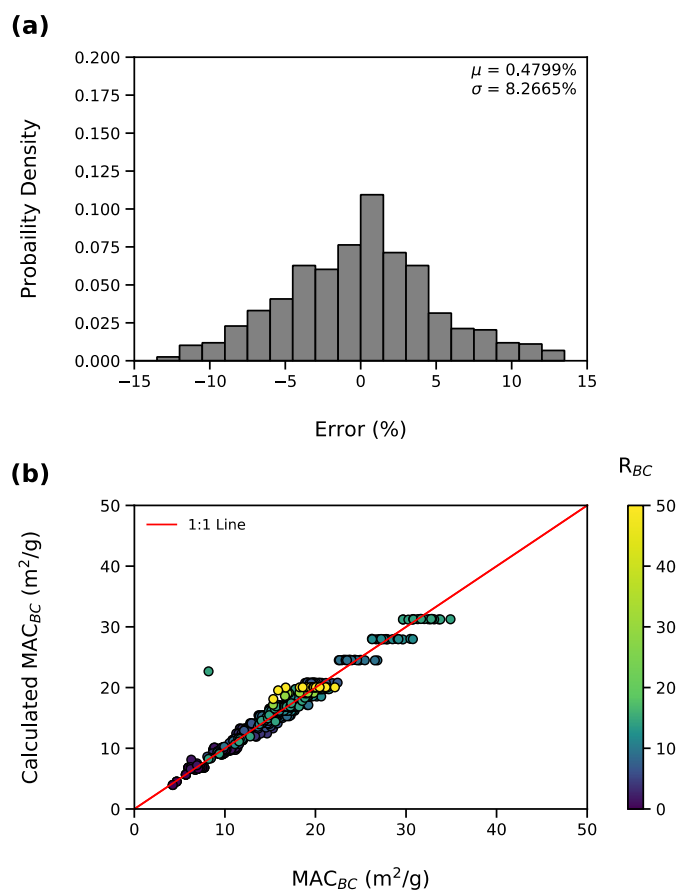


Figure 5. (a) Residual plot of fitting of equation 3. On average, equation 3 overestimates MAC_{BC} by 0.47%, with standard deviation of 8.26% (μ and σ , respectively). (b) MAC_{BC} calculated using equation 3 as a function of MAC_{BC} from ADDA. Equation 3 accurately predicts MAC_{BC} from the mixing state and morphology of the BC aggregates used to develop equation 3, but relative errors increase with increased R_{BC} . It should be noted that the outlier point is a thickly coated aggregate with $\rho_{BC} \gg 1$ and $\kappa_{coat} > 0.00$, representing the limitations of the developed framework.
 215

Table 1. Value of constants used for fitting of MAC_{BC}.

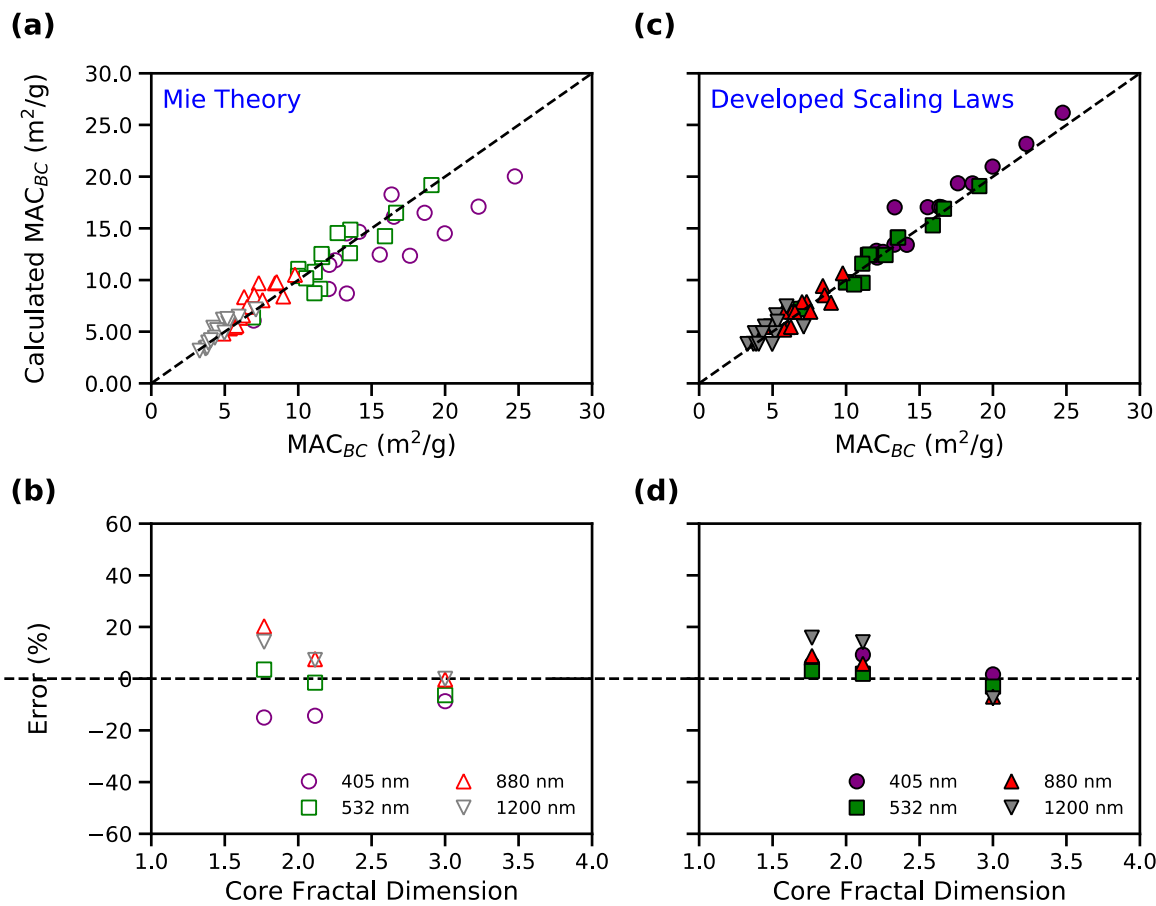
Constant	Value	95% CI
A	-1.189	0.029
B	-0.674	0.006
C	0.043	0.0007
d₁	5.679	0.027
d₂	1.066	0.058
d₃	0.264	0.010
d₄	11.421	0.137
e₁	2.440	0.017
e₂	0.593	0.024
e₃	0.418	0.020
e₄	10.106	0.131
MAC₀ (m²/g)	6.819	0.131
AAE	1.158	0.028

220

3.3 Wavelength dependency and limitations of core-shell Mie theory

Coated BC is conventionally modeled with a core-shell morphology, using Mie theory to calculate its light absorption properties (Bond and Bergstrom, 2006). Our results indicate that misrepresentation of BC morphology will inevitably lead to errors in calculation of its light absorbing properties. To highlight this point, Figure 6 compares the accuracy equation 3 in

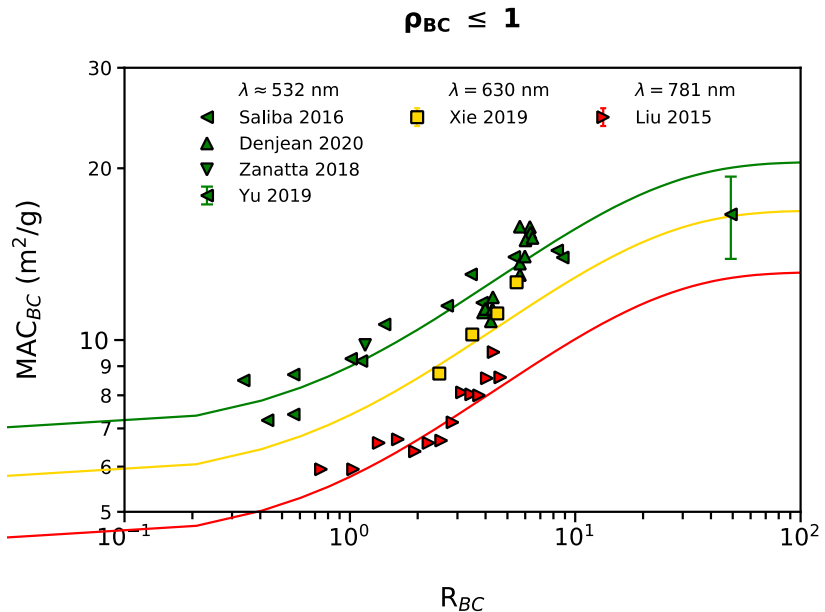
225 calculating MAC_{BC} of 15 randomly selected aggregates with $\lambda = 405$ nm, 532 nm, 880 nm, and 1200 nm to Mie theory calculations for mass-equivalent spheres (with $\kappa_{coat} = 0.00$). Figure 6 shows that across wavelengths, equation 3 accurately calculates MAC_{BC}, with average error of $9.08 \pm 10.94\%$. Figure 6 also shows that Mie theory is inconsistent in calculating MAC_{BC} for aggregates with fractal morphologies ($D_f \neq 3.0$). Figure 6b shows that Mie theory overestimates MAC_{BC} at long wavelengths and underestimates MAC_{BC} at shorter wavelengths. These results are consistent with previous findings that Mie
230 theory overestimates absorption by BC, given that BC absorption is commonly measured at longer wavelengths to avoid absorption by organic coatings (Cappa et al., 2019; Fierce et al., 2020). We also find that the accuracy of Mie Theory improves significantly as D_f approaches 3, which is analogous to the morphology of BC approaching that of a sphere. Conversely, equation 3 is more consistent in calculating MAC_{BC} with any morphology. It should be noted that the development of equation 3 involved only data points for $\lambda = 532$ nm. However, previous work has shown that enhancement of MAC_{BC} is independent
235 of λ (Chakrabarty and Heinson, 2018), indicating that results obtained for $\lambda = 532$ nm are applicable to other wavelengths. Therefore, Figure 6 (c-d) also shows the utility of equation 3 in calculating MAC_{BC} across wavelengths.



240 **Figure 6.** (a-b) MAC_{BC} calculated using Mie theory (calculated MAC_{BC}) as a function of MAC_{BC}, and error incurred by using Mie theory as a function of core fractal dimension (D_f) (c-d) MAC_{BC} calculated using equation 3 (calculated MAC_{BC}) as a function of MAC_{BC}, and error incurred by using equation 3 as a function of D_f . In panels (b) and (d), the shaded region shows the range of errors (one standard deviation). The scaling laws given in this work are more consistent than Mie theory in calculating MAC_{BC} for aggregates with arbitrary morphology.

3.4 Validation of scaling laws with field and laboratory observations

245 Figure 7(a) shows the scaling of MAC_{BC} with R_{BC} for aggregates with $\rho_{BC} \leq 1$, along with data from studies which find significant increases of MAC_{BC} with increasing R_{BC} (Yu et al., 2019; Saliba et al., 2016; Liu et al., 2015; Xie et al., 2019; Denjean et al., 2020; Zanatta et al., 2018). We find that MAC_{BC} from these studies closely matches the behavior of equation 3a, indicating that these studies were measuring light absorption properties of aggregates with $\rho_{BC} \leq 1$. It has been hypothesized that large values of MAC_{BC} in these studies could be the result of absorbing coatings. However, we find that the data from 250 these studies closely matches scaling of MAC_{BC} with κ_{coat} fixed at 0.00. The assumption that $\kappa_{coat} = 0.00$ is bolstered by the fact that refractory organics absorb preferentially at ultraviolet wavelengths (Chakrabarty et al., 2010; Sumlin et al., 2018; Kirchstetter et al., 2004; Sengupta et al., 2018; Shamjad et al., 2018), and we have only included data from visible and near-infrared wavelengths.



255

Figure 7. Scaling of MAC_{BC} with R_{BC} for aggregates with $\rho_{BC} \leq 1$ (equation 3a, solid lines), compared to the findings of several other studies which find significant MAC_{BC} (Yu et al., 2019; Saliba et al., 2016; Liu et al., 2015; Xie et al., 2019; Denjean et al., 2020; Zanatta et al., 2018). We find that measurements from these studies are well described by equation 3a, indicating that the aggregates measured in these studies had $\rho_{BC} \leq 1$.

260

Study	Wavelength (nm)	ρ_{BC}
Cappa 2012	532	2.3 ± 0.38
Cui 2016	678	1.7 ± 0.27
Cappa 2019	532	2.6 ± 0.22
Shiraiwa 2010	532	1.8 ± 0.69
Zhang 2018	880	1.5 ± 0.31

265

Table 2. Previous studies which find little to no increase in MAC_{BC} with increasing R_{BC} , and the corresponding average ρ_{BC} which replicates the measured MAC_{BC} . Using equation 3b, we are able to estimate ρ_{BC} of aggregates from studies which find values of MAC_{BC} which are significantly lower than that predicted by equation 3a (Cappa et al., 2012; Shiraiwa et al., 2010; Cappa et al., 2019; Zhang et al., 2018; Cui et al., 2016). Error in ρ_{BC} is one standard deviation.

270

Figure 7(b) shows a table of previous studies which find little to no increase in MAC_{BC} with increasing R_{BC} , and the corresponding average ρ_{BC} which replicates the measured MAC_{BC} . The average ρ_{BC} was found by solving equation 3b, inserting each measured R_{BC} and corresponding MAC_{BC} . The importance of ρ_{BC} in estimation of MAC_{BC} is evident when comparing experimentally-measured MAC_{BC} for different studies shown in Table 2. For example, Cappa et al. 2019 sampled coated BC aggregates in Fontana and Fresno, California, and find little to no increase in MAC_{BC} , even with $R_{BC} > 10$ (Cappa et al., 2019). They postulate that the low value of MAC_{BC} is due to unequal distribution of coating material between BC particles. Separate studies have shown that uneven distribution of coating can cause decreased MAC_{BC} , but thorough consideration of heterogeneous coating amounts fails to fully explain low MAC_{BC} observed in the field (Fierce et al., 2020). Therefore, our results suggest that elevated ρ_{BC} due to core restructuring may be partially responsible for low MAC_{BC} observed

275

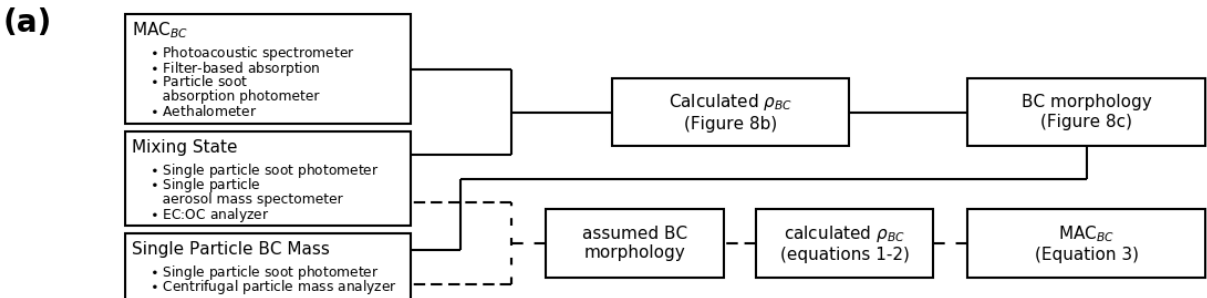
by Cappa *et al.* 2019, further highlighting the importance of the diversity of BC morphology *and* mixing state in estimation of its light absorption properties.

3.5 Applications of the developed framework

The scaling laws given in this work allow experimentalists to carry out two procedures. The first is the forward procedure, where experimentally-measured BC mass, mixing state, and coating refractive index are combined with assumed BC morphology, and MAC_{BC} is calculated. The second is the inverse procedure, where experimentally-measured BC mass, mixing state, and MAC_{BC} are inputs and BC morphology is output. Further, the inverse and forward procedures can be combined to estimate κ_{coat} . We have developed an open-source python package, called the ‘python BC absorption package’ (pyBCabs), which performs the forward and inverse functions. The following sections provide a brief overview of pyBCabs, as well as examples of inverse problems and estimation of κ_{coat} . Further details regarding the functionality of the package, as well as more examples of forward and inverse problems for single BC particles and distributions of BC particles can be found at <https://pybcabs.readthedocs.io/en/latest/index.html>.

3.5.1 Forward procedure for light absorption properties

In the forward procedure, experimentally measured R_{BC} and single particle BC mass are first combined with the assumed morphology of BC and κ_{coat} . Then, ρ_{BC} is calculated using equations 1 and 2, based on the assumed morphology and BC mass. Finally, MAC_{BC} is calculated using equation 3(a) or 3(b). A flowchart of the forward procedure is shown by the dashed lines in Figure 8(a). As an example, a fresh BC particle with mass-equivalent diameter of 300 nm and $R_{BC} = 3.68$ is input to the forward procedure along with the wavelength of interest (405 nm), and $MAC_{BC} = 16.703 \text{ m}^2/\text{g}$ is output. A BC particle with the same characteristics of the previous example, but with a fully collapsed BC core would have MAC_{BC} of 11.46 m^2/g . This example demonstrates the utility of the developed framework in evaluating changes in MAC_{BC} as coating-induced restructuring occurs during atmospheric processing.



(b)

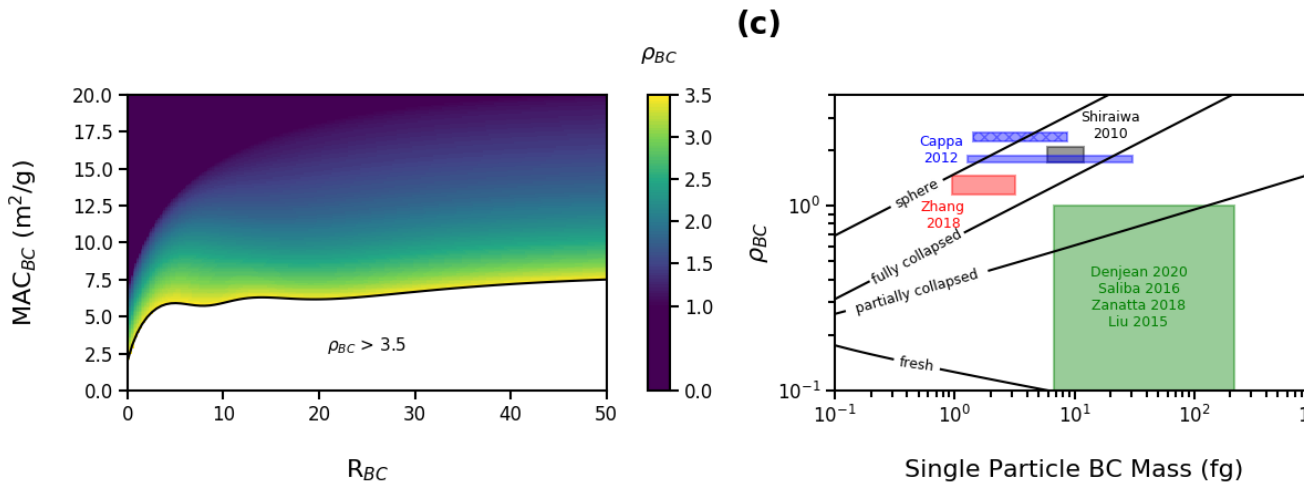


Figure 8. (a) Flowchart for forward (dashed lines) and inverse (solid lines) procedures of python BC absorption module (pyBCabs), which uses three measured properties: mass absorption cross-section (MAC_{BC}), coating amount (R_{BC}), and single particle BC mass. In the forward procedure, the assumed BC morphology is combined with the single particle BC mass to calculate MAC_{BC} (dashed lines). In the inverse procedure (solid lines), measurements of MAC_{BC} and R_{BC} are first input to panel (b) in order to constrain the core phase shift parameter (ρ_{BC}). Then, ρ_{BC} and the single particle BC mass are input to panel (c) to estimate the BC core structure. This procedure has been carried out for data from three studies, and find that low MAC_{BC} from these studies can be explained by extensive compaction of the BC core (Cappa et al., 2012; Shiraiwa et al., 2010; Zhang et al., 2018). The procedure outlined in panel (a) has also been carried out for data from several studies which found significant increases in MAC_{BC} with increasing R_{BC}, and find that the core morphology lies between fresh and partially collapsed (Saliba et al., 2016; Liu et al., 2015; Denjean et al., 2020; Zanatta et al., 2018). The examples shown here are all calculated assuming κ_{coat} = 0.00.

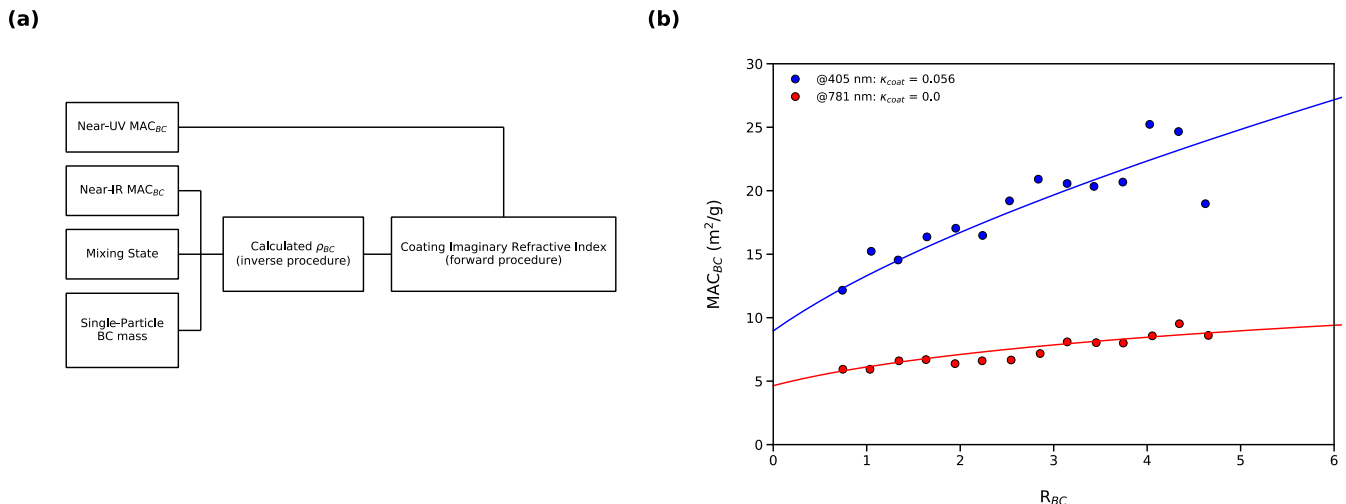
3.5.2 Inverse procedure for morphology retrieval

In the inverse procedure, experimentally measured R_{BC} and κ_{coat} is first input to equation 3a, and MAC_{BC} is calculated. If the calculated MAC_{BC} replicates the measured MAC_{BC}, then it can be concluded that the measured BC has ρ_{BC} ≤ 1, but the exact ρ_{BC} cannot be determined. If the measured MAC_{BC} is much less than that predicted by equation 3a, then Figure 8 (b) can be used to estimate ρ_{BC}. Alternatively, equation 3b can be used to calculate ρ_{BC} directly. Finally, the single particle BC mass and ρ_{BC} are combined with Figure 8 (c) to give insight to how much restructuring the BC core has undergone. A flowchart of the inverse procedure is shown by the solid lines in Figure 8 (a). The inverse procedure has been carried out for 7 previous studies (Cappa et al., 2012; Saliba et al., 2016; Shiraiwa et al., 2010; Liu et al., 2015; Zhang et al., 2018; Denjean et al., 2020; Zanatta et al., 2018)

et al., 2018), and the results are shown in Figure 8 (c). Our results indicate that studies which find little to no increase in MAC_{BC} with increased R_{BC} may be measuring BC aggregates which have undergone significant coating-induced restructuring, leading to $\rho_{BC} > 1$, and may also be measuring particles which have significant heterogeneity in R_{BC} . On the other hand, studies that find significant increases in MAC_{BC} may be measuring aggregates which have $\rho_{BC} < 1$. This does not imply that these 320 studies are measuring BC which has not restructured, only that the product of the size parameter and core packing fraction of BC is not large enough such that $\rho_{BC} > 1$.

3.5.3 Inverse procedure for coating refractive index retrieval

The inverse and forward procedures can be combined to estimate κ_{coat} , if MAC_{BC} is measured at multiple wavelengths. To accomplish this, ρ_{BC} is first found using the inverse procedure outlined above, using MAC_{BC} measured at a near-infrared wavelength (where κ_{coat} can be estimated as 0.00). Then, ρ_{BC} , R_{BC} , and MAC_{BC} can be used to solve for κ_{coat} at near-ultraviolet and visible wavelengths. This procedure is outlined in Figure 9 (a), and has been carried out for Liu *et al.*'s 2015 study, which measured absorption enhancement for BC which was internally mixed with absorbing organics (Liu *et al.*, 2015). We estimate that for this study, $\kappa_{coat} = 0.056$ at $\lambda = 405$ nm. Figure 9 (b) shows data collected by Liu *et al.* at $\lambda = 781$ nm (red points) and $\lambda = 405$ nm (blue points). The solid lines show MAC_{BC} calculated using equation 3, inserting the appropriate λ and κ_{coat} . Our 325 estimation of κ_{coat} is slightly greater than the reported κ_{coat} in Liu *et al.* However, Liu *et al.* approximated κ_{coat} using Rayleigh-Debye-Gans approximations, not direct measurement (Liu *et al.*, 2015). Additionally, our estimation of κ_{coat} is consistent with previous studies of refractive index of absorbing organics (Chakrabarty *et al.*, 2010; Sumlin *et al.*, 2018; Kirchstetter *et al.*, 330 2004; Sengupta *et al.*, 2018; Shamjad *et al.*, 2018).



335

Figure 9. (a) Flowchart for estimation of coating refractive index. First, ρ_{BC} is determined using the inverse procedure with MAC_{BC} measured at near-infrared (near-IR) wavelength, where coating imaginary refractive index (κ_{coat}) can be estimated as 0.00. Then, MAC_{BC} at near near-ultraviolet (near-UV) wavelength and calculated ρ_{BC} are input to equation 3 and κ_{coat} is calculated using the forward procedure. (b) Example of coating imaginary refractive index retrieval for

340 Liu et al. 2015 (Liu et al., 2015). First, measured MAC_{BC} at $\lambda = 781$ is used to retrieve BC morphology. We find that the BC in this study close matches scaling of MAC_{BC} with $\rho_{BC} \leq 1$. Once ρ_{BC} is known, measured mixing state and MAC_{BC} at $\lambda = 405$ are input to equation 3a and κ_{coat} is solved for. We estimate that κ_{coat} at $\lambda = 405$ is approximately 0.056. Data points show measurements made by Liu *et al.* and solid lines show result of equation 3 with appropriate κ_{coat} and λ .

4 Conclusions

345 This study comprehensively investigates the effect of BC morphology on light absorption, introduces ρ_{BC} as a central parameter in accurate estimation of MAC_{BC} , and develops improved scaling laws for MAC_{BC} . We find that for aggregates with $\rho_{BC} \leq 1$, MAC_{BC} increases with increasing R_{BC} . For aggregates with $\rho_{BC} > 1$, MAC_{BC} is a function of R_{BC} and ρ_{BC} . Our work also shows that as ρ_{BC} increases past unity, MAC_{BC} decreases. We then provide a comparison of the scaling laws presented in this work with Mie theory calculations for mass-equivalent spheres. We find that Mie theory consistently overestimates MAC_{BC} of 350 internally mixed BC with $\rho_{BC} > 1$, which is consistent with previous studies which also find that Mie theory greatly overestimates absorption by BC (Cappa et al., 2012, 2019; Fierce et al., 2020). The scaling laws presented in this work account for the microphysical properties of BC, and provide a new tool for estimating BC light absorption based on BC morphology.

355 Finally, we validate our findings with data from 11 previous studies which measure light absorption enhancement (Yu et al., 2019; Cappa et al., 2012; Saliba et al., 2016; Shiraiwa et al., 2010; Liu et al., 2015; Cappa et al., 2019; Zhang et al., 2018; Xie et al., 2019; Denjean et al., 2020; Zanatta et al., 2018; Cui et al., 2016). We find that studies which find significant absorption enhancement with increasing R_{BC} agree well with our scaling laws for BC with $\rho_{BC} \leq 1$ (Saliba et al., 2016; Liu et al., 2015; Denjean et al., 2020; Zanatta et al., 2018; Xie et al., 2019; Yu et al., 2019). We also find that $\rho_{BC} > 1$ is a possible explanation for studies which find little to no absorption enhancement (Cappa et al., 2012; Shiraiwa et al., 2010; Cappa et al., 2019; Zhang et al., 2018; Cui et al., 2016). These findings are significant because coating-induced restructuring of the BC core will lead to 360 increases in the core packing fraction, and consequent increases in ρ_{BC} . Our findings suggest that restructuring of the BC core and increased ρ_{BC} can lead to decreased absorption, and may play a role in previous discrepancies in measured MAC_{BC} . Previous work has shown that heterogeneity in BC mixing state accounts for a large portion of the discrepancies in measured and modeled BC, but does not fully reconcile previous discrepancies in BC absorption. Our study shows that particle-resolved mixing state and detailed representation of BC morphology are both necessary in order to fully parameterize absorption by 365 internally mixed BC.

370 In order to make the results of this study readily available to experimentalists, we conclude by providing an open-source Python module, the ‘python BC absorption package’ (pyBCabs). This package has two functionalities. The first functionality is for forward problems, where BC mass and R_{BC} of ambient and laboratory generated BC are input, and MAC_{BC} is returned. The second functionality is for inverse problems, where BC mass, R_{BC} , and MAC_{BC} of ambient and laboratory generated BC are input, and the morphology of BC is returned. The forward and inverse functionalities can also be combined to estimate the imaginary part of the coating refractive index, if MAC_{BC} is measured at multiple wavelengths.

375 The inverse functionality of this module allows for in-situ inference of BC morphology, as opposed to ex-situ methods of determining BC morphology, such as electron microscopy. Use of the inverse functionality of pyBCabs will allow for more detailed studies on the evolution of BC morphology during its atmospheric lifetime. Improved representation of BC morphology, as well as the improved scaling laws developed by this study can then be incorporated into radiative transfer models, and eventually aid in reducing the uncertainty of radiative forcing by carbonaceous aerosols.

380

Data availability. All data from ADDA calculations are available for download at https://github.com/beelerpayton/ADDA_datasets. Full details regarding the functionality of the developed python package can be found at <https://pybcabs.readthedocs.io/en/latest/index.html>.

385 **Supplement.** Includes methods for converting absorption enhancement from previous field and laboratory studies to mass absorption cross-section. Also includes two figures showing examples of a modelled partially collapsed BC particle (S1), and data used for calculation of absorption Ångstrom exponent (S2).

390 **Author contributions.** RKC and PB conceived of the study and its design. RKC provided guidance and supervision for carrying out the research tasks, interpretation of results, and contributed to the preparation of the manuscript. PB performed the data analysis, developed the figures, and led the preparation of the manuscript. PB and RKC were involved in the editing and proofreading of the manuscript.

395 **Competing interests.** The authors declare that they have no known competing financial interests or personal relationships that could have appeared to influence the work reported in this paper.

Acknowledgements

This work was supported by the U.S. National Science Foundation (AGS-1926817), the NASA ACCDAM program (NNH20ZDA001N), and the US Department of Energy (DE-SC0021011). Funding for collecting data during the 2010 CARES field campaign in California was provided by the Atmospheric Radiation Measurement (ARM) Program sponsored by the US 400 Department of Energy (DOE), Office of Biological and Environmental Research (OBER). The authors thank Dr. William Heinson for insightful comments and assisting with getting this project off the ground.

References

Bond, T. C. and Bergstrom, R. W.: Light Absorption by Carbonaceous Particles: An Investigative Review, *Aerosol Science and Technology*, 40, 27–67, <https://doi.org/10.1080/02786820500421521>, 2006.

405 Bond, T. C., Doherty, S. J., Fahey, D. W., Forster, P. M., Berntsen, T., DeAngelo, B. J., Flanner, M. G., Ghan, S., Kärcher, B., Koch, D., Kinne, S., Kondo, Y., Quinn, P. K., Sarofim, M. C., Schultz, M. G., Schulz, M., Venkataraman, C., Zhang, H., Zhang, S., Bellouin, N., Guttikunda, S. K., Hopke, P. K., Jacobson, M. Z., Kaiser, J. W., Klimont, Z., Lohmann, U., Schwarz, J. P., Shindell, D., Storelvmo, T., Warren, S. G., and Zender, C. S.: Bounding the role of black carbon in the climate system: A scientific assessment: BLACK CARBON IN THE CLIMATE SYSTEM, *J. Geophys. Res. Atmos.*, 118, 5380–5552, 410 <https://doi.org/10.1002/jgrd.50171>, 2013.

Boucher, O., Balkanski, Y., Hodnebrog, Ø., Myhre, C. L., Myhre, G., Quaas, J., Samset, B. H., Schutgens, N., Stier, P., and Wang, R.: Jury is still out on the radiative forcing by black carbon, *Proc Natl Acad Sci USA*, 113, E5092–E5093, <https://doi.org/10.1073/pnas.1607005113>, 2016.

415 Cappa, C. D., Onasch, T. B., Massoli, P., Worsnop, D. R., Bates, T. S., Cross, E. S., Davidovits, P., Hakala, J., Hayden, K. L., Jobson, B. T., Kolesar, K. R., Lack, D. A., Lerner, B. M., Li, S.-M., Mellon, D., Nuaaman, I., Olfert, J. S., Petaja, T., Quinn, P. K., Song, C., Subramanian, R., Williams, E. J., and Zaveri, R. A.: Radiative Absorption Enhancements Due to the Mixing 420 State of Atmospheric Black Carbon, *Science*, 337, 1078–1081, <https://doi.org/10.1126/science.1223447>, 2012.

Cappa, C. D., Zhang, X., Russell, L. M., Collier, S., Lee, A. K. Y., Chen, C.-L., Betha, R., Chen, S., Liu, J., Price, D. J., Sanchez, K. J., McMeeking, G. R., Williams, L. R., Onasch, T. B., Worsnop, D. R., Abbatt, J., and Zhang, Q.: Light Absorption 425 by Ambient Black and Brown Carbon and its Dependence on Black Carbon Coating State for Two California, USA, Cities in Winter and Summer, *J. Geophys. Res. Atmos.*, 124, 1550–1577, <https://doi.org/10.1029/2018JD029501>, 2019.

Chakrabarty, R. K. and Heinson, W. R.: Scaling Laws for Light Absorption Enhancement Due to Nonrefractory Coating of Atmospheric Black Carbon Aerosol, *Phys. Rev. Lett.*, 121, 218701, <https://doi.org/10.1103/PhysRevLett.121.218701>, 2018.

425 Chakrabarty, R. K., Moosmüller, H., Chen, L.-W. A., Lewis, K., Arnott, W. P., Mazzoleni, C., Dubey, M. K., Wold, C. E., Hao, W. M., and Kreidenweis, S. M.: Brown carbon in tar balls from smoldering biomass combustion, *Atmos. Chem. Phys.*, 10, 6363–6370, <https://doi.org/10.5194/acp-10-6363-2010>, 2010.

Chen, C., Enekwizu, O. Y., Fan, X., Dobrzanski, C. D., Ivanova, E. V., Ma, Y., Gor, G. Y., and Khalizov, A. F.: Single parameter for predicting the morphology of atmospheric black carbon, *Environmental science & technology*, 52, 14169–14179, 2018.

430 China, S., Mazzoleni, C., Gorkowski, K., Aiken, A. C., and Dubey, M. K.: Morphology and mixing state of individual freshly emitted wildfire carbonaceous particles, *Nat Commun*, 4, 2122, <https://doi.org/10.1038/ncomms3122>, 2013.

Cui, X., Wang, X., Yang, L., Chen, B., Chen, J., Andersson, A., and Gustafsson, Ö.: Radiative absorption enhancement from 435 coatings on black carbon aerosols, *Science of The Total Environment*, 551–552, 51–56, <https://doi.org/10.1016/j.scitotenv.2016.02.026>, 2016.

Debye, P. P.: *Light Scattering by Small Particles*. HC Van de Hulst. Wiley, New York; Chapman & Hall, London, 1957. xiii+470 pp. Illus. \$12., *Science*, 127, 477–478, 1958.

Denjean, C., Brito, J., Libois, Q., Mallet, M., Bourrianne, T., Burnet, F., Dupuy, R., Flamant, C., and Knippertz, P.: Unexpected Biomass Burning Aerosol Absorption Enhancement Explained by Black Carbon Mixing State, *Geophys. Res. Lett.*, 47, <https://doi.org/10.1029/2020GL089055>, 2020.

440 Fierce, L., Onasch, T. B., Cappa, C. D., Mazzoleni, C., China, S., Bhandari, J., Davidovits, P., Al Fischer, D., Helgestad, T., and Lambe, A. T.: Radiative absorption enhancements by black carbon controlled by particle-to-particle heterogeneity in composition, *Proceedings of the National Academy of Sciences*, 117, 5196–5203, 2020.

Gustafsson, Ö. and Ramanathan, V.: Convergence on climate warming by black carbon aerosols, *Proc Natl Acad Sci USA*, 113, 4243–4245, <https://doi.org/10.1073/pnas.1603570113>, 2016.

445 Heinson, W. R. and Chakrabarty, R. K.: Fractal morphology of black carbon aerosol enhances absorption in the thermal infrared wavelengths, *Opt. Lett.*, 41, 808, <https://doi.org/10.1364/OL.41.000808>, 2016.

Heinson, W. R., Liu, P., and Chakrabarty, R. K.: Fractal scaling of coated soot aggregates, *Aerosol Science and Technology*, 51, 12–19, 2017.

450 Hu, K., Liu, D., Tian, P., Wu, Y., Deng, Z., Wu, Y., Zhao, D., Li, R., Sheng, J., and Huang, M.: Measurements of the diversity of shape and mixing state for ambient black carbon particles, *Geophysical Research Letters*, 48, e2021GL094522, 2021.

Hu, K., Liu, D., Tian, P., Wu, Y., Li, S., Zhao, D., Li, R., Sheng, J., Huang, M., and Ding, D.: Identifying the Fraction of Core–Shell Black Carbon Particles in a Complex Mixture to Constrain the Absorption Enhancement by Coatings, *Environmental Science & Technology Letters*, 2022.

455 Kirchstetter, T. W., Novakov, T., and Hobbs, P. V.: Evidence that the spectral dependence of light absorption by aerosols is affected by organic carbon: SPECTRAL LIGHT ABSORPTION BY AEROSOLS, *J. Geophys. Res.*, 109, n/a-n/a, <https://doi.org/10.1029/2004JD004999>, 2004.

460 Liu, D., Whitehead, J., Alfarra, M. R., Reyes-Villegas, E., Spracklen, D. V., Reddington, C. L., Kong, S., Williams, P. I., Ting, Y.-C., Haslett, S., Taylor, J. W., Flynn, M. J., Morgan, W. T., McFiggans, G., Coe, H., and Allan, J. D.: Black-carbon absorption enhancement in the atmosphere determined by particle mixing state, *Nature Geosci.*, 10, 184–188, <https://doi.org/10.1038/ngeo2901>, 2017.

Liu, F., Yon, J., Fuentes, A., Lobo, P., Smallwood, G. J., and Corbin, J. C.: Review of recent literature on the light absorption properties of black carbon: Refractive index, mass absorption cross section, and absorption function, *Aerosol Science and Technology*, 54, 33–51, 2020.

465 Liu, S., Aiken, A. C., Gorkowski, K., Dubey, M. K., Cappa, C. D., Williams, L. R., Herndon, S. C., Massoli, P., Fortner, E. C., Chhabra, P. S., Brooks, W. A., Onasch, T. B., Jayne, J. T., Worsnop, D. R., China, S., Sharma, N., Mazzoleni, C., Xu, L., Ng, N. L., Liu, D., Allan, J. D., Lee, J. D., Fleming, Z. L., Mohr, C., Zotter, P., Szidat, S., and Prévôt, A. S. H.: Enhanced light absorption by mixed source black and brown carbon particles in UK winter, *Nat Commun.*, 6, 8435, <https://doi.org/10.1038/ncomms9435>, 2015.

470 Lu, Z., Streets, D. G., Winijkul, E., Yan, F., Chen, Y., Bond, T. C., Feng, Y., Dubey, M. K., Liu, S., and Pinto, J. P.: Light absorption properties and radiative effects of primary organic aerosol emissions, *Environmental science & technology*, 49, 4868–4877, 2015.

Meakin, P.: Formation of Fractal Clusters and Networks by Irreversible Diffusion-Limited Aggregation, *Phys. Rev. Lett.*, 51, 1119–1122, <https://doi.org/10.1103/PhysRevLett.51.1119>, 1983.

475 Meakin, P.: Fractal aggregates, *Advances in Colloid and Interface Science*, 28, 249–331, [https://doi.org/10.1016/0001-8686\(87\)80016-7](https://doi.org/10.1016/0001-8686(87)80016-7), 1987.

Peng, J., Hu, M., Guo, S., Du, Z., Zheng, J., Shang, D., Levy Zamora, M., Zeng, L., Shao, M., Wu, Y.-S., Zheng, J., Wang, Y., Glen, C. R., Collins, D. R., Molina, M. J., and Zhang, R.: Markedly enhanced absorption and direct radiative forcing of black carbon under polluted urban environments, *Proc Natl Acad Sci USA*, 113, 4266–4271, <https://doi.org/10.1073/pnas.1602310113>, 2016.

480 Reidmiller, D., Avery, C., Easterling, D., Kunkel, K., Lewis, K., Maycock, T., and Stewart, B.: Fourth national climate assessment, Volume II: Impacts, risks, and adaptation in the United States, Washington, DC, USA: US Global Change Research Program, 2018.

485 Romshoo, B., Müller, T., Pfeifer, S., Saturno, J., Nowak, A., Ciupek, K., Quincey, P., and Wiedensohler, A.: Optical properties of coated black carbon aggregates: numerical simulations, radiative forcing estimates, and size-resolved parameterization scheme, *Atmospheric Chemistry and Physics*, 21, 12989–13010, 2021.

Saliba, G., Subramanian, R., Saleh, R., Ahern, A. T., Lipsky, E. M., Tasoglou, A., Sullivan, R. C., Bhandari, J., Mazzoleni, C., and Robinson, A. L.: Optical properties of black carbon in cookstove emissions coated with secondary organic aerosols: Measurements and modeling, *Aerosol Science and Technology*, 50, 1264–1276, <https://doi.org/10.1080/02786826.2016.1225947>, 2016.

490 Sengupta, D., Samburova, V., Bhattacharai, C., Kirillova, E., Mazzoleni, L., Iaukea-Lum, M., Watts, A., Moosmüller, H., and Khlystov, A.: Light absorption by polar and non-polar aerosol compounds from laboratory biomass combustion, *Atmos. Chem. Phys.*, 18, 10849–10867, <https://doi.org/10.5194/acp-18-10849-2018>, 2018.

Shamjad, P., Satish, R., Thamban, N. M., Rastogi, N., and Tripathi, S.: Absorbing refractive index and direct radiative forcing of atmospheric brown carbon over Gangetic Plain, *Acs Earth and Space Chemistry*, 2, 31–37, 2018.

495 Shetty, N., Beeler, P., Paik, T., Brechtel, F. J., and Chakrabarty, R. K.: Bias in quantification of light absorption enhancement of black carbon aerosol coated with low-volatility brown carbon, *Aerosol Science and Technology*, 55, 539–551, 2021.

Shiraiwa, M., Kondo, Y., Iwamoto, T., and Kita, K.: Amplification of Light Absorption of Black Carbon by Organic Coating, *Aerosol Science and Technology*, 44, 46–54, <https://doi.org/10.1080/02786820903357686>, 2010.

Sorensen, C. and Fischbach, D.: Patterns in Mie scattering, *Optics Communications*, 173, 145–153, 2000.

500 Sorensen, C. M.: Light Scattering by Fractal Aggregates: A Review, *Aerosol Science and Technology*, 40, 2001.

Sumlin, B. J., Heinson, Y. W., Shetty, N., Pandey, A., Pattison, R. S., Baker, S., Hao, W. M., and Chakrabarty, R. K.: UV–Vis–IR spectral complex refractive indices and optical properties of brown carbon aerosol from biomass burning, *Journal of Quantitative Spectroscopy and Radiative Transfer*, 206, 392–398, <https://doi.org/10.1016/j.jqsrt.2017.12.009>, 2018.

505 Wang, Y., Liu, F., He, C., Bi, L., Cheng, T., Wang, Z., Zhang, H., Zhang, X., Shi, Z., and Li, W.: Fractal Dimensions and Mixing Structures of Soot Particles during Atmospheric Processing, *Environ. Sci. Technol. Lett.*, 4, 487–493, <https://doi.org/10.1021/acs.estlett.7b00418>, 2017.

Xie, C., Xu, W., Wang, J., Liu, D., Ge, X., Zhang, Q., Wang, Q., Du, W., Zhao, J., Zhou, W., Li, J., Fu, P., Wang, Z., Worsnop, D., and Sun, Y.: Light absorption enhancement of black carbon in urban Beijing in summer, *Atmospheric Environment*, *Atmospheric Environment*, 213, 499–504, <https://doi.org/10.1016/j.atmosenv.2019.06.041>, 2019.

510 Yu, P., Toon, O. B., Bardeen, C. G., Zhu, Y., Rosenlof, K. H., Portmann, R. W., Thornberry, T. D., Gao, R.-S., Davis, S. M., Wolf, E. T., de Gouw, J., Peterson, D. A., Fromm, M. D., and Robock, A.: Black carbon lofted wildfire smoke high into the stratosphere to form a persistent plume, *Science*, 365, 587–590, <https://doi.org/10.1126/science.aax1748>, 2019.

Yurkin, M. A. and Hoekstra, A. G.: The discrete-dipole-approximation code ADDA: Capabilities and known limitations, *Journal of Quantitative Spectroscopy and Radiative Transfer*, 112, 2234–2247, <https://doi.org/10.1016/j.jqsrt.2011.01.031>, 2011.

Zanatta, M., Laj, P., Gysel, M., Baltensperger, U., Vratolis, S., Eleftheriadis, K., Kondo, Y., Dubuisson, P., Winiarek, V., Kazadzis, S., Tunved, P., and Jacobi, H.-W.: Effects of mixing state on optical and radiative properties of black carbon in the European Arctic, *Atmos. Chem. Phys.*, 18, 14037–14057, <https://doi.org/10.5194/acp-18-14037-2018>, 2018.

520 Zangmeister, C. D., Radney, J. G., Dockery, L. T., Young, J. T., Ma, X., You, R., and Zachariah, M. R.: Packing density of rigid aggregates is independent of scale, *Proceedings of the National Academy of Sciences*, 111, 9037–9041, 2014.

Zhang, Y., Favez, O., Canonaco, F., Liu, D., Močnik, G., Amodeo, T., Sciare, J., Prévôt, A. S. H., Gros, V., and Albinet, A.: Evidence of major secondary organic aerosol contribution to lensing effect black carbon absorption enhancement, *npj Clim Atmos Sci*, 1, 47, <https://doi.org/10.1038/s41612-018-0056-2>, 2018.